Tellus (1989), *41A*, 18–31

Efficient dynamical initialization of a limited area model

By ARNE M. BRATSETH, *Institute of Geophysics, University of Oslo P.O. Box 1022 Blindern, 0315 Oslo 3, Norway*

(Manuscript received 18 September 1987; in final form 25 April 1988)

ABSTRACT

The dynamical initialization used in the limited area weather prediction routine at the Norwegian Meteorological Institute is presented. 3 iterations, corresponding to 6 model time steps, are shown to produce an almost noise-free integration. This efficient noise reduction is achieved by means of simple filters which cause the damping rate to depend on horizontal and vertical scales as well as frequency. Normal mode arguments are used to adjust parameters so that modes moving faster than about 70 ms^{-1} are suppressed, while modes moving slower than about 30 ms^{-1} are retained. Explicit knowledge of the normal modes is not required. Implementation of the scheme is very simple, and it is easily adapted to most existing models.

1. Introduction

Modern numerical weather prediction models are able to simulate a large variety of motion systems, including high-frequency oscillations which receive very little energy in the real atmosphere. These waves are usually termed gravity waves, although some of them are dominated by acoustic and inertial effects. Due to inaccurate initial states, and to a smaller extent inaccurate models, these waves often occur with unrealistic amplitudes in numerical simulations. In order to solve this problem, a number of more-or-less successful initialization methods have been suggested, including the non-linear normal mode initialization of Machenhauer (1977) and Baer and Tribbia (1977) which appear to have gained greatest popularity in later years.

In this paper, we are going to describe a simple alternative which is used in a limited area weather prediction routine at the Norwegian Meteorological Institute. The method uses ideas suggested in Bratseth (1982), and can be described as a dynamical initialization in which the convergence rate has been enhanced by means of information about the normal modes. Complete knowledge of the normal modes is not required, however, and the method is therefore well suited to situations in which the normal modes are difficult to compute. A typical example of this is provided by the present model which is defined in a rectangular area on a polar stereographic map. In the following sections, we shall discuss the theory behind the method, the details of its implementation and its effect in a realistic data assimilation situation.

2. Basic ideas

Let the model be represented by

$$\frac{\mathrm{d}}{\mathrm{d}t}\underset{\sim}{Z}=\underset{\sim}{F}(\underset{\sim}{Z}), \tag{1}$$

where the vector $\underset{\sim}{Z}$ describes the state of the system. From the initial state $\underset{\sim}{Z}_0$ we make two forward time steps of length Δt:

$$\begin{aligned}\underset{\sim}{Z}_1&=\underset{\sim}{Z}_0+\Delta t\underset{\sim}{F}(\underset{\sim}{Z}_0),\\ \underset{\sim}{Z}_2&=\underset{\sim}{Z}_1+\Delta t\underset{\sim}{F}(\underset{\sim}{Z}_1).\end{aligned} \tag{2}$$

The second-order time derivative of $\underset{\sim}{Z}$ can now be estimated, and a new initial state with reduced high frequency noise may be computed by:

$$\underset{\sim}{Z}_0^{\mathrm{new}}=\underset{\sim}{Z}_0+\gamma\Delta^2\underset{\sim}{Z}, \tag{3}$$

where

$$\Delta^2\underset{\sim}{Z}=\underset{\sim}{Z}_2-2\underset{\sim}{Z}_1+\underset{\sim}{Z}_0, \tag{4}$$

and γ is a properly chosen constant.

In order to study the effect of this procedure, we shall write:

$$\underset{\sim}{Z} = \sum_m c_m(t)\,\underset{\sim}{Z}_m, \tag{5}$$

where the $\underset{\sim}{Z}_m$'s are normal modes of a linearized version of the model. This linear model may be expressed as a set of uncoupled equations:

$$\frac{\mathrm{d}}{\mathrm{d}t} c_m = -i\omega_m c_m, \tag{6}$$

where ω_m is the eigen-frequency of mode m. When our iteration procedure is applied, the response is:

$$c_m^{\text{new}} = (1 - \gamma\omega_m^2 \Delta t^2) c_m. \tag{7}$$

For $\gamma\omega_m^2\Delta t^2 = 1$, the mode will vanish, while for $\gamma\omega_m^2\Delta t^2 > 2$ or $\gamma\omega_m^2\Delta t^2 < 0$, the mode will be amplified.

In Bratseth (1982), the same response function was obtained by using the truncation error in a forward-backward integration cycle as suggested by Nitta (1969). Similar effects may of course be produced in many different ways, and the trick should be easy to adapt to most existing models.

This type of response function has some severe shortcomings when used for initialization purposes. The constant γ has to be chosen small enough to prevent divergence for the fastest mode of the system. Usually we also want to suppress modes with much lower frequencies, and for these modes $\gamma\omega^2\Delta t^2$ will be too small to provide efficient damping. Furthermore, the damping rate should probably not be a function of frequency alone. Slow meteorological waves with short wavelengths may have frequencies equal to, or higher than those of fast gravity waves with long wavelengths. In Bratseth (1982) it was suggested to improve the response function by using different γ's for different modes, and this is the approach to be investigated in the following.

Before we go on to work out the details of the method, it is appropriate to be more specific about what we want to achieve. What types of motions do we want to suppress, and why? In the full non-linear system the normal modes are governed by equations of the form:

$$\frac{\mathrm{d}}{\mathrm{d}t} c + i\omega c = r, \tag{8}$$

where r represents all the terms that were left out in the linearization. Let us assume that the non-linear forcing r has a variation in time which is characterized by a typical frequency ω_r. If ω_r is comparable to the frequency of free oscillations ω, then resonant interactions are possible and large transient oscillations may take place. If, however, ω_r is much smaller than ω, very little energy is transferred to such oscillations, and the time behaviour of c will be characterized by ω_r rather than by ω. In this way, we may explain why gravity waves with phase speeds much larger than typical advective speeds are hard to find in the real atmosphere. The thermal forcing which drives atmospheric motions varies too slowly to produce such transients by direct interaction. Furthermore, due to the limited strength of the forcing, the generated meteorological motions are also too slow to be efficient in this respect. The existence of short meteorological waves with frequencies similar to long gravity waves does not change this picture. The non-linear forcing of a mode of a certain scale will be dominated by modes with similar structures and we can therefore assume that the relevant ω_r characterizes meteorological systems of this scale.

Our goal should be to suppress oscillations which cannot be expected to have an efficient natural generating mechanism. The identification of such modes should depend not only on the frequency, but also on the structure in space. As a convenient single indicator we choose the phase speed, and we define our goal to be to suppress waves which propagate much faster than typical meteorological systems. The speed of meteorological systems seldom exceeds 20 ms^{-1}. Certainly, strong jet streams are several times faster than this, but in our problem it is the motion of systems and not air parcels which matters. Ultra-long planetary waves are known to propagate with very high speeds (Eliasen and Machenhauer, 1969), and might need some special care. However, in the regional model that we are dealing with in the present paper, we are not going to try to suppress such long waves. Roughly speaking, our aim will be to suppress waves which are faster than about 70 ms^{-1}, and to retain waves which are slower than about 30 ms^{-1}.

At this stage, it is appropriate to review some basic facts about inertial gravity waves. If we linearize the shallow water equations about a state of rest, and introduce perturbations of the form $\exp[i(kx - \omega t)]$, we find inertial gravity wave solutions with frequencies:

$$\omega = \pm(gHk^2 + f^2)^{1/2}. \tag{9}$$

Here H is the average depth, g is the acceleration of gravity and f is the Coriolis-parameter which is assumed to be constant. A wave moving in the x-direction then has the phase speed:

$$c = \pm(c_g^2 + c_f^2)^{1/2}, \tag{10}$$

where $c_g^2 = gH$ and $c_f^2 = f/k$.

These considerations are relevant to three-dimensional primitive equation models of the atmosphere. When these models are linearized about a state of rest, the equations can be transformed into a number of shallow water problems with different equivalent depths (see for instance Temperton and Williamson, 1981), which increase with increasing vertical wavelength. The corresponding values of c_g range from almost zero to about 300 ms^{-1}.

In Fig. 1, the phase speed c is shown as a function of c_g and c_f, The inertial velocity c_f is proportional to the horizontal wavelength, and a length scale, assuming $f = 10^{-4}\ \mathrm{s}^{-1}$, is therefore included. It is seen that there exist a wide range of wave solutions which should be suppressed according to our criteria. Furthermore, the included frequency isolines show that a damping which depends only on frequency is inadequate for our purposes. Finally Fig. 1 can also be used to illustrate the limitations of initialization methods based on geostrophy. Such methods can be expected to work only when the Rossby number $R = Uk/f = U/c_f$ is much smaller than unity, i.e., when c_f is much larger than a typical fluid velocity U.

If a dynamical initialization of the type (3) is to be used, we obviously need a different γ for each mode. To provide this, we shall try to replace the constant γ by an operator $\underset{\sim}{\Gamma}$ so that (3) is replaced by:

$$\underset{\sim}{Z}_0^{\text{new}} = \underset{\sim}{Z}_0 + \underset{\sim}{\Gamma}(\Delta^2 \underset{\sim}{Z}). \tag{11}$$

Clearly, if the normal modes of the model are known explicitly, an operator with ideal properties can be constructed. In recent years normal modes have been computed for a number

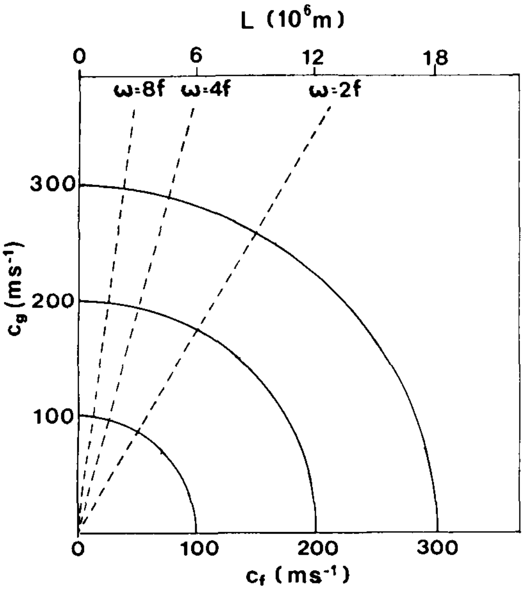

Fig. 1. Phase speed (full lines) and frequency (dashed lines) of inertial gravity waves as functions of c_f (or L) and c_g.

of models, mainly for use in non-linear normal mode initialization (see for instance Temperton and Williamson, 1981). The model to be initialized in the present paper uses polar stereographic map coordinates, which do not allow the normal mode problem to be separated in the two horizontal dimensions. The computation and manipulation of normal modes of such a model are excessively time-consuming, and we shall have to choose another approach. Brière (1982) has shown that modes of a simplified f-plane model in Cartesian coordinates can be used in normal mode initialization of certain limited area models. Such modes may be useful in our case too. However, large groups of modes require fairly similar γ's, and it therefore seems unnecessary to carry out a complete modal decomposition. Instead we shall investigate the potential of a simple operator which performs a rather crude separation of different horizontal scales and vertical structures.

3. Horizontal separation

We have chosen to use discrete bandpass filters based on the operators:

$$X_n\alpha_{ij} = \tfrac{1}{2}\alpha_{ij} + \tfrac{1}{4}(\alpha_{i+n,j} + \alpha_{i-n,j}),$$
$$Y_n\alpha_{ij} = \tfrac{1}{2}\alpha_{ij} + \tfrac{1}{4}(\alpha_{ij+n} + \alpha_{ij-n}), \tag{12}$$

where n is a natural number, and α_{ij} is a function defined on a regular grid. Fields of increasing smoothness can be generated by:

$$S_1\alpha = X_1 Y_1 \alpha,$$
$$S_2\alpha = X_2 Y_2 S_1 \alpha,$$
$$S_4\alpha = X_4 Y_4 S_2 \alpha, \tag{13}$$
$$\ldots\ldots\ldots$$
$$S_n\alpha = X_n Y_n S_{n/2} \alpha.$$

Here n is assumed to be of the form $n = 2^m$ where m is a natural number. For notational convenience we shall also make the definition $S_{1/2}\alpha = \alpha$.

When S_n is applied to a wave component of the form $\alpha = \exp[i(kx + ly)]$ on a grid with meshwidth h, we get a response function R_n which may be generated by:

$$R_{1/2} = 1,$$
$$R_n = \cos^2(nkh/2)\cos^2(nlh/2)R_{n/2}. \tag{14}$$

Fig. 2 shows R_n as a function of $K = (k^2 + l^2)^{1/2}$

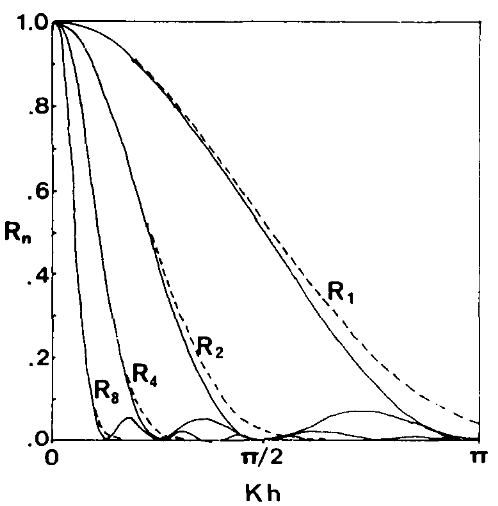

Fig. 2. Response function R_n as a function of $Kh = (k^2 + l^2)^{1/2}h$ when $l = 0$ (full lines) and $l = k$ (dashed lines)

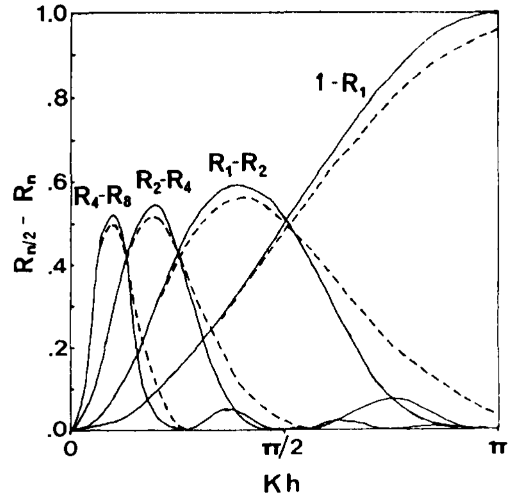

Fig. 3. Response function $R_{n/2} - R_n$ as a function of $Kh = (k^2 + l^2)^{1/2}h$, when $l = 0$ (full lines) and $l = k$ (dashed lines).

when $l = 0$ (full line), and when $k = l$ (dashed line). Closer inspection shows that R_n is almost independent of the direction of the wavenumber vector. A general two-dimensional field may now be decomposed in the following way;

$$\alpha = (\alpha - S_1\alpha) + (S_1\alpha - S_2\alpha) + \ldots + (S_{N/2}\alpha - S_N\alpha) + S_N\alpha. \tag{15}$$

Each parenthesis on the right of (15) represents, in a rough way, a certain band of wavelengths. The characteristic wavelength increases with increasing degree of smoothing, and the final term contains the remaining large scales. From Fig. 3, which shows the response of $S_{n/2} - S_n$, we can estimate a characteristic wavenumber k_n for each of the components in (15). Assuming that c_g and f are known, we can use (9) to compute a suitable ω_n and a suitable value of γ by:

$$\gamma_n = (\omega_n \Delta t)^{-2}. \tag{16}$$

The operator Γ may now be defined by:

$$\Gamma(\alpha) = \sum_{m=0}^{M} \gamma_n (S_{n/2} - S_n)\alpha + \gamma_R S_N \alpha, \tag{17}$$

with $n = 2^m$ and $N = 2^M$.

4. Vertical separation

In the vertical, it is convenient to characterize the normal modes and the corresponding shallow water systems by their order (Temperton and Williamson, 1981); the order being a natural number which increases with increasing vertical complexity (as measured for instance by the number of nodes). The equivalent depth and the phase speed will decrease systematically with increasing order. In our method a separation along these lines may be used to speed up the convergence. The second order time derivatives estimated by (4) can be transformed so that the contribution from each shallow water system can be found. The horizontal operator (17) can then be applied to each vertical component with γ's based on the appropriate equivalent depth.

Although this approach is possible with our model, it seems unnecessary to perform this detailed analysis of the vertical structure. In order to stress simplicity we shall instead try a very simple approach which is more in line with our crude horizontal separation. The idea is to split $\Delta^2 \underset{\sim}{Z}$ in two parts, a low order part which represents the vertically averaged motion, and a high order part which represents the deviation from the vertical average.

The model to be initialized is a σ-surface model with prognostic variables:

$\underset{\sim}{v}(x,y,\sigma,t)$ horizontal velocity
$\theta(x,y,\sigma,t)$ potential temperature
$p_s(x,y,t)$ surface pressure

The vertical coordinate is defined as:

$$\sigma = \frac{p - p_T}{p_s - p_T},$$

where p_T is a constant which defines the top of the model atmosphere. We define the low order contribution to be:

$$\begin{aligned}
&\Delta^2 \underset{\sim}{v}^{(L)} = \int_0^1 \Delta^2 \underset{\sim}{v}\, d\sigma, \\
&\Delta^2 \theta^{(L)} = 0, \qquad\qquad (19)\\
&\Delta^2 p_s^{(L)} = \Delta^2 p_s.
\end{aligned}$$

The high-order part is then simply:

$$\begin{aligned}
&\Delta^2 \underset{\sim}{v}^{(H)} = \Delta^2 \underset{\sim}{v} - \Delta^2 \underset{\sim}{v}^{(L)}, \\
&\Delta^2 \theta^{(H)} = \Delta^2 \theta, \qquad\qquad (20)\\
&\Delta^2 p_s^{(H)} = 0.
\end{aligned}$$

The choice for θ and p_s is motivated by the continuity equation in σ-coordinates:

$$\frac{\partial}{\partial t} p_s + \nabla \cdot [(p_s - p_T)\underset{\sim}{v}] + (p_s - p_T)\frac{\partial}{\partial \sigma}\dot{\sigma} = 0, \qquad (21)$$

where $\dot{\sigma} = d\sigma/dt$. When this equation is integrated in the vertical, using the boundary conditions $\dot{\sigma} = 0$ at $\sigma = 0$ and $\sigma = 1$, we get:

$$\frac{\partial}{\partial t} p_s + \nabla \cdot [(p_s - p_T)\underset{\sim}{v}^{(L)}] = 0, \qquad (22)$$

showing that it is natural to connect p_s to the low order part. Furthermore, when $\underset{\sim}{v}^{(L)}$ is inserted in (21) we find that $\dot{\sigma} = 0$ everywhere for this type of motion. The vertical advection of θ then vanishes, and θ is essentially unchanged by low-order oscillations (at least when the equations are linearized about a state of rest). This justifies the definition $\Delta^2 \theta^{(L)} = 0$.

With this splitting our operator takes the form:

$$\Gamma(\alpha) = \sum_{l = L,H} \left(\sum_{m=0}^{M} \gamma_n^{(l)}(S_{n/2} - S_n)\alpha^{(l)} + \gamma_R^{(l)} S_n \alpha^{(l)} \right), \qquad (23)$$

with $n = 2^m$ and $N = 2^M$. As one would expect from normal mode theory, the high order part turns out to be characterized by much slower motions (a smaller $c_g = (gH)^{1/2}$) than the low-order part, and allows much larger γ's without causing divergence of the iteration procedure.

5. Implementation

5.1. *The model*

As already mentioned, the model to be initialized is a limited area sigma surface model, defined inside a rectangular area on a polar stereographic map. In the horizontal a regular grid of 61 × 49 points is used, with a meshwidth of 150 km at 60° of latitude. The integration area is shown in Fig. 4. Horizontal differencing is based on the scheme called TSDM in Bratseth (1983). The model has its top ($\sigma = 0$) at $p_T = 100$ hPa, and the atmosphere below is divided in ten layers of equal mass ($\Delta\sigma = 0.1$). The variables u, v and θ are defined in the middle of these layers, and $\dot{\sigma} = d\sigma/dt$ is defined at the intersections. Second-order differencing is used for all vertical derivatives. Explicit leapfrog time integration is

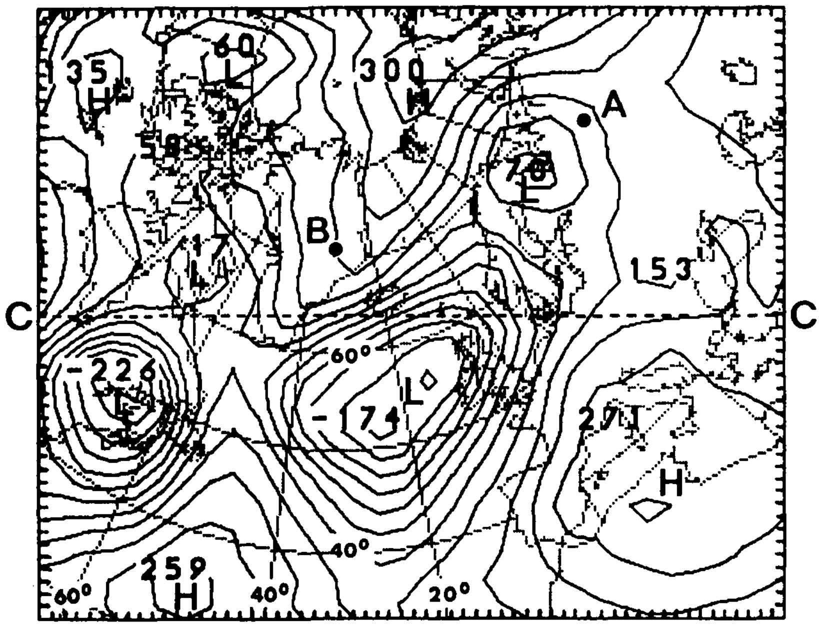

Fig. 4. Uninitialized analysis of 1000 hPa geopotential height at 00 GMT 3 December 1985. Intervals of 40 gpm.

used together with "the Shuman pressure averaging technique" as described by Brown and Campana (1978) and a time filter following Asselin (1972). The time step is 450 s. No "physics" has been included in the present experiments. Further details of an early version of the model is to be found in Grønås and Hellevik (1982).

5.2 *Lateral boundaries*

The model is equipped with boundary relaxation zones in which the prognostic variables Z' at the end of each time step are relaxed in a Newtonian fashion towards a prescribed background Z_B by means of:

$$Z = Z' - a(Z' - Z_B). \tag{24}$$

The coefficient a is a function of the distance s from the boundary, starting with $a(0) = 1$ at the boundary and decreasing to zero at $s = s_{max}$ according to

$$a(s) = 1 - (s/s_{max})^2. \tag{25}$$

The width of the relaxation zone, s_{max}, is defined to be 5 meshwidths.

Experiments have shown that the use of this relaxation zone in the initialization cycles may cause serious convergence problems. This was expected because the use of this zone produces damped waves with complex frequencies where the imaginary part may dominate over the real part. Clearly, such waves require γ's which are very different from those that we have suggested. It seems that the easiest way round this problem is to switch off the relaxation during the initialization. Therefore, during the foreward timesteps in (2) the boundary treatment is reduced to a simple specification of all variables at the boundary.

We want to use the operator $\underset{\sim}{\Gamma}$ all the way to the boundary, and this implies that we will need values at points which are outside the integration area. After some experimentation we have chosen to attack this problem by extending the fields $\Delta^2 u$, $\Delta^2 v$, $\Delta^2 \theta$ and $\Delta^2 p_s$ as anti-symmetric functions outside the boundaries, i.e., we define $\Delta^2\alpha(s) = -\Delta^2\alpha(-s)$. In principle, this can be done without any modification of $\Delta^2\alpha$ in the integration area because the specification of α at the boundary forces $\Delta^2\alpha(0)$ to be zero anyway.

However, grid points influenced by this unphysical boundary condition tend to become noisy, and we have chosen to modify the first and second grid point away from the boundary by multiplication by $\frac{1}{3}$ and $\frac{2}{3}$, respectively.

This procedure has no particular physical justification, and was chosen mainly because it appears to be stable and robust. It certainly does not guarantee a proper balance near the boundary, but this seems to be less important because much of the gravity noise in this area will be dissipated by the boundary relaxation scheme.

When the initialization is finished and the main time integration is started, it is of some importance that the background fields which are imposed by the relaxation zone, are updated to include the modification produced by the initialization. If this is not done, the fields in this zone will quickly be forced back to their original values, and this process may generate gravity waves.

5.3. Specification of parameters

In the operator (23), we have used $M = 3$ which means that the basic filters (12) are used with $n = 1$, 2, 4 and 8. The parameters $\gamma_n^{(L)}$ and $\gamma_n^{(H)}$ have been estimated by means of:

$$\gamma = (\omega \Delta t)^{-2} = (c_g{}^2 k^2 + f^2)^{-1} \Delta t^{-2}. \qquad (26)$$

Appropriate values of c_g and k (or $L = 2\pi/k$) for each term in (23) have been determined by rough guesses based on theoretical considerations, followed by a final adjustment based on experiments. By monitoring the root-mean-square of each term it is possible to get a fairly good picture of the convergence rate of each component, and each γ can to a large extent be optimized independently of the others. As one would expect, the performance of the scheme is not very sensitive to small changes in the parameters.

Unless otherwise stated, we have used the following values:

$$c_g^{(L)} = 333 \text{ ms}^{-1}, \quad c_g^{(H)} = 100 \text{ ms}^{-1},$$

$$L_1 = 5h, \quad L_2 = 5h, \quad L_4 = 10h,$$
$$L_8 = 20h, \quad L_R = 40h.$$

Here L_n is the characteristic wavelength used in γ_n, and h is the constant meshwidth of the map-coordinate grid. Ideally L_n should depend on the true meshwidth which varies over the integration area. In the present application this variation is small, and we have chosen to neglect it. The variation of the Coriolis parameter also has a very modest effect on the γ's, and we have chosen to use the constant $f = 10^{-4}\ s^{-1}$. In this way, the γ's become uniform in space. Note, however, that this simplification is not strictly necessary to the implementation of the method.

The parameter L_1 is much larger than what might have been expected from the response function in Fig. 3. This has to do with the difference scheme of the model which severely underestimates derivatives in space of the shortest waves. As a result, the simulated waves are much too slow, with frequencies similar to those of much longer waves. The effect will be different for different numerical schemes, and the optimal L_1 must be expected to be highly model dependent.

Another parameter which may be expected to be model dependent is $c_g^{(H)}$. The equivalent depths of the normal modes of numerical models depend on the details of the vertical discretization, and the value $c_g^{(H)} = 100$ ms^{-1} may turn out to be inadequate for other models.

Rough estimates of the damping rates are easily obtained from (7) and (26). When f is neglected, we find that a wave with phase-speed c will be reduced by a factor of about $1 - c^2/c_g^2$ on each iteration. With $c_g = 100$ ms^{-1} and $c = 70$ ms^{-1} this damping rate becomes 0.51 which means that the mode will vanish quickly. On the other hand $c = 30$ ms^{-1} gives the damping rate 0.91 which means that at least the main part of the wave will survive a few iterations.

6. Experiments

The method described above has been used in the data-assimilation routine at the Norwegian Meteorological Institute for several years. In order to demonstrate its effect we have made some experiments based on the uninitialized analysis of 0 GMT, 3 December 1985 as taken from this data-assimilation cycle. For later reference we include the 1000 hPa geopotential hight in Fig. 4. Results will be shown for 3 different versions of the scheme:

(A) The complete version as described above.

(B) A version similar to A but with no separation in the vertical. This is accomplished by replacing $\gamma^{(H)}$ with the corresponding $\gamma^{(L)}$ everywhere in (23).

(C) A version with neither vertical nor horizontal separation, i.e., all the γ's are equal to the smallest γ of the complete scheme.

In the following, the root mean square over the integration area of the second order time derivatives of iteration $n+1$ will be used to diagnose the situation after n iterations. Fig. 5 shows RMS $(\partial^2 p_s/\partial t^2)$ as a function of the number of iterations which has been completed. The results are in good agreement with the theoretical considerations of the previous sections. Scheme A (full line) is more efficient than scheme C (dashed line), and the rate of convergence decays very quickly as the more easily initialized modes are suppressed. Version B (dotted) is very similar to version A as far as surface pressure is concerned. For some reason B is slightly more successful than A on the first two iterations. A possible explanation is that the fastest mode is not strictly independent of hight, and some portion of it is therefore projected on the high order part. This portion is more correctly treated by scheme B than by scheme A.

Fig. 6 shows the area root mean square of $\partial^2\theta/\partial t^2$ as a function of σ. Scheme B with no vertical separation (dotted line) is seen to have much smaller impact than the full scheme A (dash-dotted) after three iterations. Ten full iterations (dashed line) lead to further noise reduction, but again the convergence rate falls off with increasing iteration number.

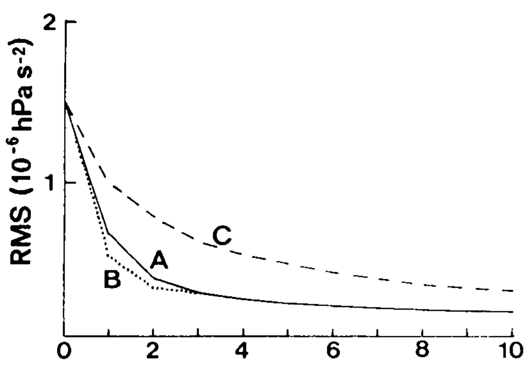

Fig. 5. Area root mean square of $\partial^2 p_s/\partial t^2$ as a function of iterations completed.

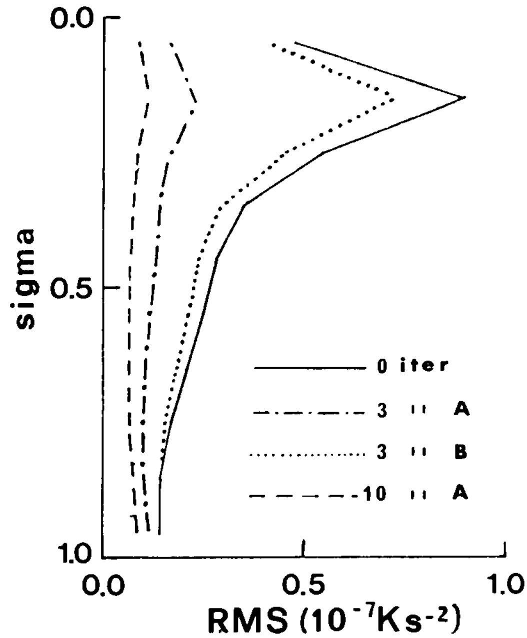

Fig. 6. Area root mean square of $\partial^2\theta/\partial t^2$ as a function of vertical coordinate (σ).

It is interesting to note that the noise in θ has a distinct maximum in the upper part of the model atmosphere, and that the noise reduction is strongest in this region also when measured in a relative sense. These observations are easily explained in light of the vertical structure of normal modes of numerical weather prediction models (see for instance Temperton and Williamson (1981)). Modes of low order (large c_g) have most of their structure and amplitude at upper levels. Due to their high frequencies, these modes contribute strongly to $\partial^2\theta/\partial t^2$, and they are easily initialized by our scheme.

So far, we have verified that we can reduce the initial second order time derivatives in agreement with our theoretical predictions. The effect on time integrations has been studied by monitoring p_s and θ in 16 gridpoints distributed over the integration area. Fig. 7 shows the surface pressure as a function of time for the point marked A in Fig. 4. Three iterations with the complete scheme (short dashes) is seen to have a very strong effect, and appears to have produced an almost noisefree integration. 10 iterations (long dashes) make very little difference, at least as far

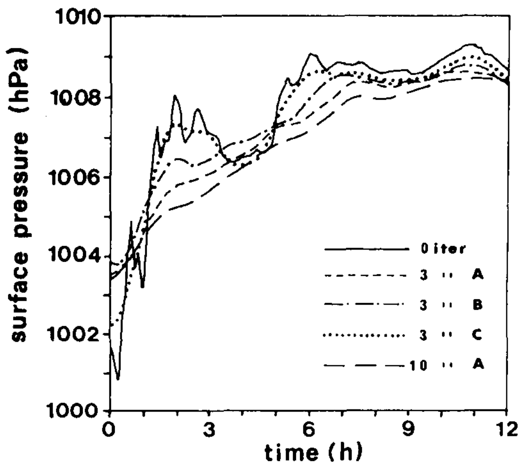

Fig. 7. Surface pressure in point A (Fig. 4) as a function of time.

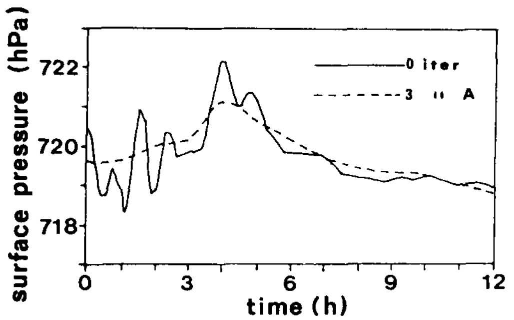

Fig. 8. Surface pressure in point B (Fig. 4) as a function of time.

as surface pressure is concerned. We have also included the result from three iterations with scheme B (dashed-dotted) and C (dotted). While B seems to be only slightly inferior to A, C is seen to fail for the longer periods. This picture is consistent with Fig. 5, and demonstrates the effect of enhanced γ's for the larger horizontal scales.

Fig. 7 is typical for the 16 points that have been inspected. In order to complete the picture we also include the point for which the initialization appears to have been least successful. This point is marked B in Fig. 4 and the result is shown in Fig. 8. The initialized curve shows a distinct deflection after about four hours. Closer inspection has shown that this feature is mainly due to a signal which starts at the boundary and propagates with a speed of about 300 ms^{-1}. Considering the rather arbitrary compromises made in the boundary zone, the existence of such waves is not surprising. The same phenomenon has been identified in other points, but with smaller amplitudes. In general we feel that these waves are so weak that they can be accepted.

In order to show that these results are representative, we include Fig. 9, which shows the surface pressure as a function of both x-coordinate and time along the line C – C in Fig. 4. To be more precise the figures show the deviation between p_s and a function which is linear in time and

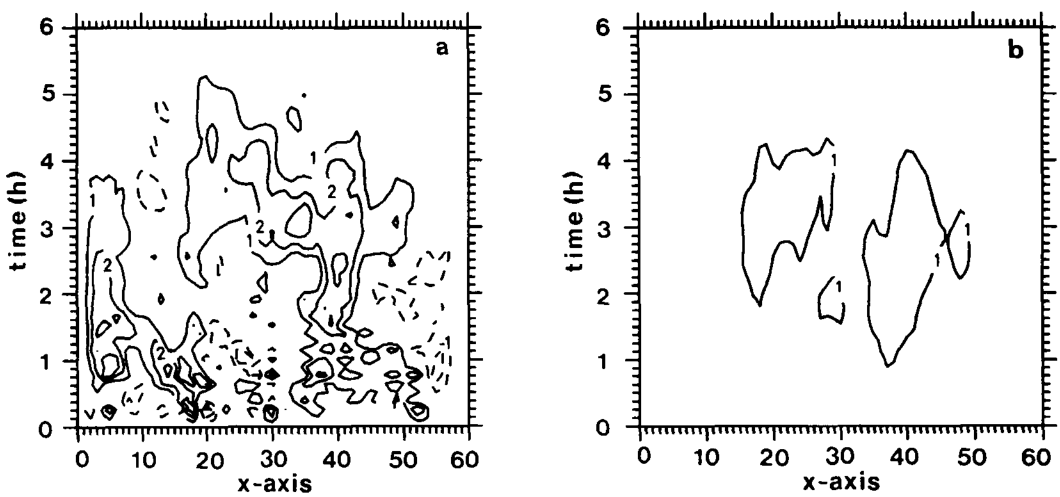

Fig. 9. Time development of the difference between surface pressure and a function linear in time (see text for details) along the line C – C in Fig. 4 (x-axis in grid units). Intervals of 1 hPa. (a) No initialization. (b) 3 iterations with scheme A.

coincides with p_s at $t = 0$ and $t = 6h$. Comparing Fig. 9a (no initialization) with Fig. 9b (3 iterations with A) we find that the noise is strongly reduced everywhere. The boundary regions which are covered by the figures do not appear to cause particular problems.

In order to visualize internal waves, we chose to concentrate on potential temperature θ as a function of time and vertical coordinate σ for the gridpoint B. Fig. 10 a, b, c and d show the difference between θ and a linear function of time which coincides with θ at $t = 0$ and $t = 12h$. Three iterations with scheme A (Fig. 10b) is seen to have a considerable impact when compared with the uninitialized case (Fig. 10a). Most notable is the suppression of an oscillation with a period of about 4 hours in the upper part of the model atmosphere. We interpret these θ-anomalies to be caused by the vertical displacements connected with an internal gravity wave of low order. This interpretation was checked against the vertical velocity ($d\sigma/dt$ – not shown). The

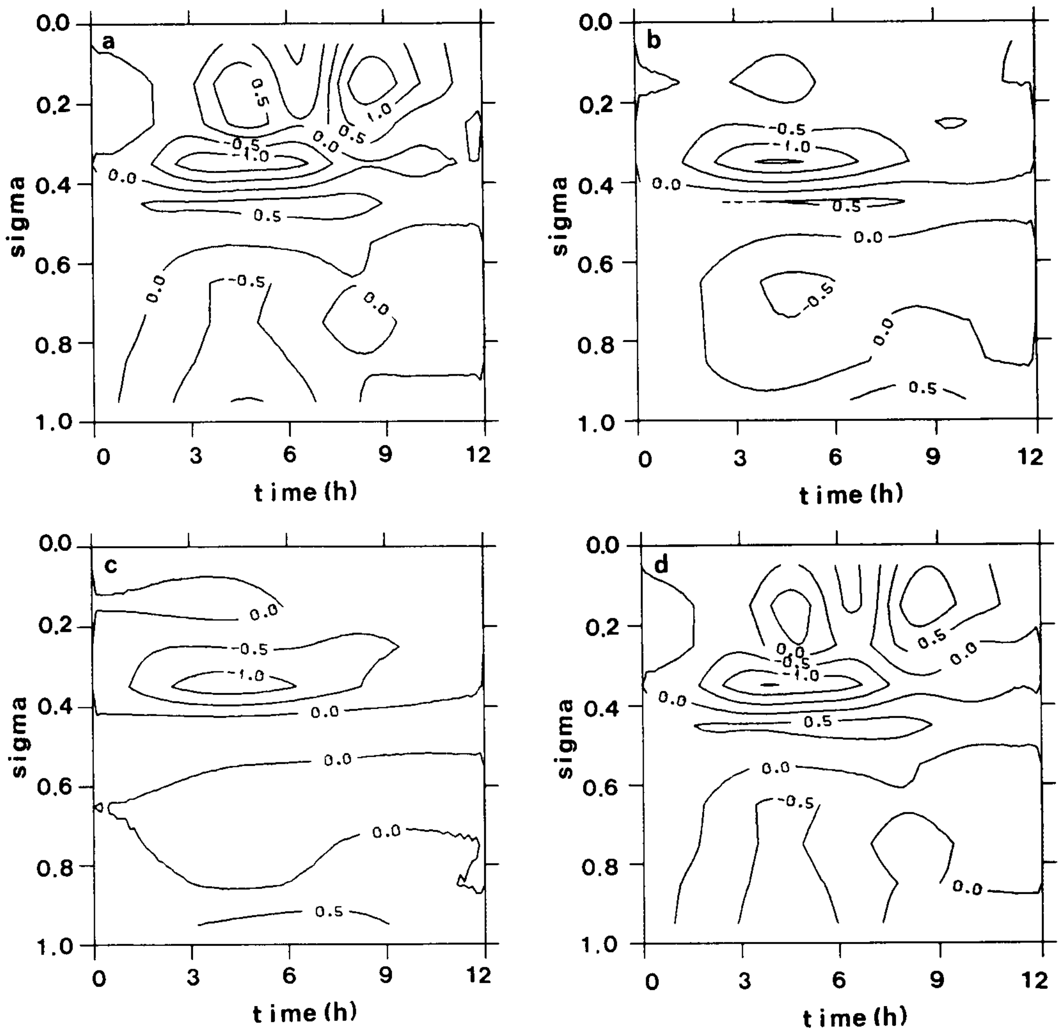

Fig. 10. Time development of the difference between potential temperature and a function linear in time (see text for details) along a vertical line in point B of Fig. 4. Intervals of 0.5°K. (a) No initialization. (b) 3 iterations with scheme A. (c) 10 iterations with scheme A. (d) 3 iterations with scheme B.

remaining features are characterized by longer timescales, and it is hard to tell whether they should be damped or not. After ten iterations (Fig. 10c) the amplitudes are further reduced. Fig. 10d on the other hand, shows that three iterations with scheme B has a very modest impact on the internal waves. This is consistent with Fig. 6, and demonstrates the effect of the vertical separation.

After this demonstration of successful noise reduction, it is appropriate to ask to what extent the initialization has changed the initial state. The RMS changes of p_s, u and θ after 3 complete iterations are 1.1 hPa, 0.8 m s^{-1} and 0.4°K, respectively. The corresponding maximum changes at a gridpoint are 4.7 hPa, 7.3 m s^{-1} and 3.2°K. These figures may not be alarming, but the maximum values are larger than current estimates of observation errors (see Hollingsworth et al., 1986), and could cause deterioration of the analysis.

Similar changes are known to follow from non-linear normal mode initialization (Puri, 1983; Williamson and Daley, 1983; Temperton, 1984). Our method is expected to remove fast gravity modes in much the same way as normal mode initialization. However, our method will also to some extent modify non-gravitational Rossby modes, and it would be interesting to know by how much this effect contributes to the total change. Because we do not have access to the normal modes, we cannot measure the effect directly. Instead we have tried to watch the time development of the difference pattern between initialized and uninitialized integrations. From this investigation it was clear that the largest differences propagated with speeds which were much larger than the speeds of the meteorological systems, and also larger than the speed of any particle of the fluid. Although the finer details were hard to interpret, we became convinced that at least in the present case the damping of the Rossby modes is a minor problem which is overshadowed by the effect on the gravity modes.

Comparison with scheme B showed that the changes in p_s were almost insensitive to the use of the vertical separation. The maximum changes in u and θ, however, were reduced substantially when this separation was not used. These changes were characterized by a very short verti-

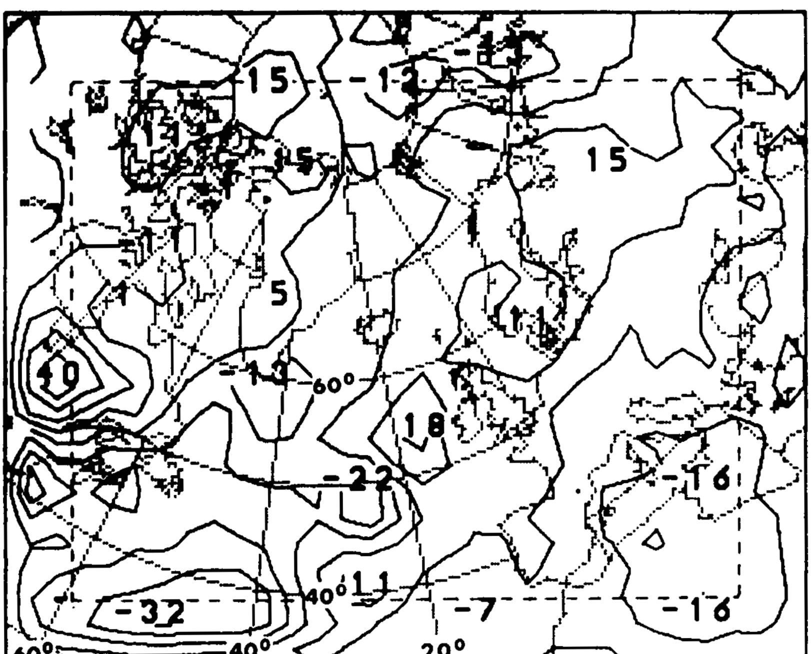

Fig. 11. Geopotential height change at 1000 hPa after 3 iterations with scheme A. Intervals of 8 gpm.

cal scale, and were located near the tropopause. It seems likely that they were caused by vertical resolution problems of some kind.

During operational use of this initialization method it has been observed that the largest changes tend to occur in the vicinity of the boundary. This also applies to the present case. As an example, we focus on the change pattern of the 1000 hPa geopotential hight after three iterations with scheme A (Fig. 11). Comparison with Fig. 4 shows that some of the largest changes coincides with a relatively intense low near the western boundary, while others are more difficult to explain. It is of course natural to suspect that the phenomenon is a consequence of the arbitrary formulation at the open boundary. However, other explanations are also possible. There are strong reasons to believe that the initial analysis is of lower quality in the boundary zone than in the interior. The data assimilation system which produced the initial state, is based on boundary values from global forecasts made at NMC, Washington. However, these forecasts have not been available in their complete form, but only in the form of geopotential heights of 1000 hPa, 700 hPa, 500 hPa, 300 hPa and 100 hPa in a $5^0 \times 5^0$ grid at 12 hour intervals. These data are interpolated to the model grid and winds are computed geostrophically. The analysis is based on a first guess which consists of a six hour forecast. The boundary zone of this first guess is strongly influenced by the low quality boundary fields, and it is likely that the boundary zone of the final analysis will contain more gravitational noise than the interior.

In order to check the effect of the boundary we have made an experiment in a smaller area with boundaries placed five grid-lengths inside the original boundaries (dashed line in Fig. 11). Fig. 12 together with Fig. 11 show that the position of the boundary has only a modest effect on the changes made in the smaller area. This indicates that the occurrence of maximum changes in the boundary zone is a property of the initial state rather than of the initialization method.

7. Possible extension

In Bratseth (1982), it was suggested to conserve meteorological modes by keeping certain terms constant during each iteration cycle. This trick

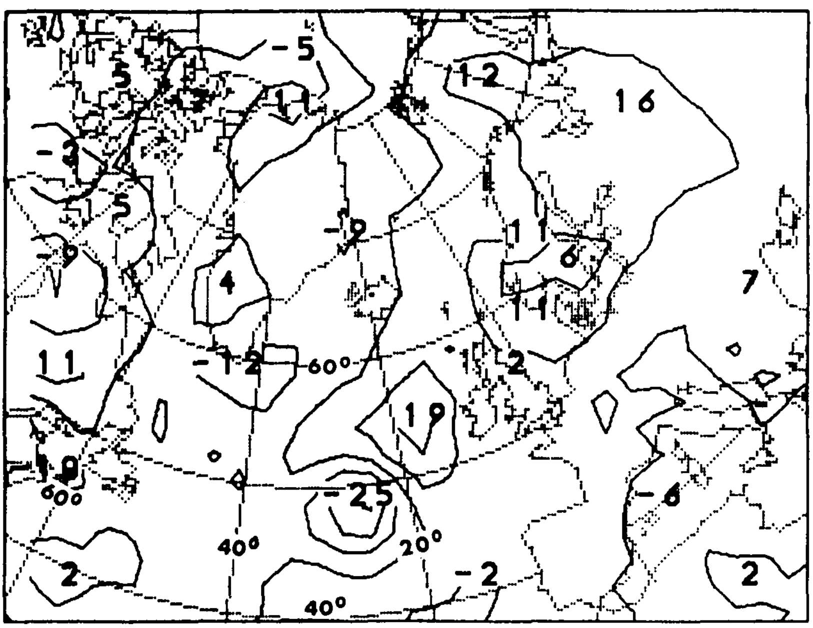

Fig. 12. Same as Fig. 11, but with new boundary along the dashed line of Fig. 11.

applies to the present situation as well. If the non-linear forcing r of (8) is kept constant during a complete cycle, then (7) should be replaced by:

$$c^{\text{new}} = (1 - \gamma\omega^2\Delta t^2)c - i\gamma\omega\Delta t^2 r, \qquad (27)$$

If r is linearized to give $r = -i\omega_r c$, we get:

$$c^{\text{new}} = (1 - \gamma\omega(\omega + \omega_r)\Delta t^2)c, \qquad (28)$$

in contrast to

$$c^{\text{new}} = (1 - \gamma(\omega + \omega_r)^2\Delta t^2)c, \qquad (29)$$

which applies to the experiments above. Clearly, meteorological modes for which ω is much smaller than ω_r will be much less influenced by (28) than by (29). A simple example is discussed in Bratseth (1982).

We have not tried to apply this device in the present model. Its application would require a certain reprogramming of the model, so that the advection terms could be stored and used in several time steps. Considering that the damping of meteorological modes seems to represent a minor contribution to the total changes, we have not found it worthwhile to pursue this idea. Clearly, if the initialization is to be constrained to follow the observations, something quite different is needed, like for instance the analysis-initialization cycle discussed by Williamson and Daley (1983).

Another point to consider is a more detailed separation of modes. Normal mode schemes often initialize modes of somewhat higher order than what has been attempted with the present method, sometimes with $c_g < 50$ ms^{-1}. Our high order part with $c_g = 100$ ms^{-1} will have some effect on such modes. However, to initialize these modes efficiently we would have to use a finer vertical separation so that smaller and more appropriate values of c_g could be used. Inevitably we would then do more harm to the meteorological modes, and it might be necessary to protect them by means of the device described above. To our knowledge the value of suppressing such modes has never been demonstrated, and we have decided not to pursue the problem.

As for the horizontal resolution we have found no need to improve it neither by Fourier-techniques nor by including more terms in (17). Experiments with different γ's in (17) have shown that the contribution of the largest scale is small, and the operator could in fact have been made even simpler without losing much of its effect. In general, it is to be expected that the more severe inconsistencies in the analysis are of a relatively small scale, reflecting resolution problems of the observation network, and to a smaller extent of the model.

8. Concluding remarks

In this paper, it has been demonstrated that, in addition to the model itself, simple filter operators are all that is needed for a quite efficient noise suppression in a limited area model. We have not made any comparison with other initialization schemes, but it seems likely that the more important effects of a normal mode initialization can be reproduced with this simple method. An advantage of this approach is that it can be used even when normal modes are hard to find and manipulate, although normal mode initialization with approximate modes will often work. The strongest argument in favour of the method is probably its simple implementation, and it should therefore represent an interesting alternative to modelling groups with limited man-power resources to spend on the initialization problem.

9. Acknowledgements

This work was supported by the Norwegian Meteorological Institute. In particular we want to thank Sigbjørn Grønås for many useful discussions.

REFERENCES

Asselin, R. 1972. Frequency filter for time integrations. *Mon. Wea. Rev. 100*, 487–490.

Baer, F. and Tribbia, J. 1977. On complete filtering of gravity modes through non-linear initialization. *Mon. Wea. Rev. 105*, 1536–1539.

Bratseth, A. M. 1982. A simple and efficient approach to the initialization of weather prediction models. *Tellus, 34*, 352–357.

Bratseth, A. M. 1983. Some economical, explicit finit difference schemes for the primitive equations. *Mon. Wea. Rev. 111*, 663–668.

Brière, S. 1982. Non-linear normal mode initialization of a limited-area model. *Mon. Wea. Rev. 110*, 1166–1186.

Brown, H. A. and Campana, K. A. 1978. An economical time-differencing system for numerical weather prediction. *Mon Wea. Rev. 106*, 1025–1036.

Eliasen, E. and Machenhauer, B. 1969. On the observed large-scale atmospheric wave motion. *Tellus 21*, 149–166.

Grønås, S. and Hellevik, O. E. 1982. A limited area prediction model at the Norwegian Meteorological Institute. *Technical Report No. 61*, Det Norske Meteorologiske Institutt, 75 pp.

Hollingsworth, A., Shaw, D. B. Lönnberg, P., Illari, L., Arpe, K. and Simmons, A. J. 1986. Monitoring of Observation and Analysis Quality by a Data Assimilation System. *Mon. Wea. Rev. 114*, 861–879.

Machenhauer, B. 1977. On the dynamics of gravity oscillations in a shallow water model, with application to normal mode initialization. *Contrib. Atmos. Phys. 50*, 253–271.

Nitta, T. 1969. Initialization and analysis for the primitive equation model. *Proc. of the WMO/IUGG Synposium on Num. Wea. Pred., Vol. VI*, 11–20. Tokyo, Japan, 1968.

Puri, K. 1983. Some experiments in variational normal mode initialization in data assimilation. *Mon. Wea. Rev. 111*, 1208–1218.

Temperton, C. and Williamson, D. L. 1981. Normal mode initialization for a multilevel grid-point model, I, Linear aspects, *Mon. Wea. Rev. 104*, 729–743.

Temperton, C. 1984. Variational normal mode initialization for a multilevel model. *Mon. Wea. Rev. 107*, 2303–2316.

Williamson, D. L. and Daley, R. 1983. A unified analysis-initialization technique. *Mon. Wea. Rev. 111* 1517–1536.